J Adv Ceram

Research Article

A novel efficient preparation route for BN matrix composites reinforced with Al_2O_3 fibers based on textured design

Bo Wang[1,2], Delong Cai[3,✉], Xiaoming Duan[1,2], Zhihua Yang[1,2], Daxin Li[1,2], Zhenxi Lu[4], Dechang Jia[1,2,✉], Yu Zhou[1,2,5]

Cite this article: Wang B, Cai D, Duan X, et al. *J Adv Ceram* 2026, **15**(3): 9221246. https://doi.org/10.26599/JAC.2026.9221246

ABSTRACT: Conventional boron nitride (BN)-based composites are often limited by high porosity and long processing cycles, which severely restrict their mechanical performance and engineering applications. To overcome these limitations, a novel organic–inorganic hybrid matrix combined with a hot-compression orientation strategy is proposed. Liquid-phase polyborazylene (PBZ) was employed to promote the rearrangement and alignment of *h*-BN lamellae during pressing, and subsequent pyrolysis yielded a dense and continuous BN matrix with in situ precipitated nanocrystals serving as load-transfer nodes. This process significantly enhanced densification, reduced porosity, and enabled the construction of an ordered lamellar structure. Unlike conventional PIP processes that typically require ~10 repeated infiltration–pyrolysis cycles, this method achieves dense composites in a single pyrolysis step, effectively avoiding fiber damage and greatly shortening the fabrication cycle. The synergistic effects of aligned lamellae inducing extended crack propagation paths and in situ nanocrystals providing additional load-transfer mechanisms effectively improved the mechanical performance of the composites. The proposed PBZ-assisted hybrid matrix and lamellar-orientation design strategy offers a new and efficient route for developing high-performance BN-based composites with excellent wave-transmitting and thermal protection capabilities.

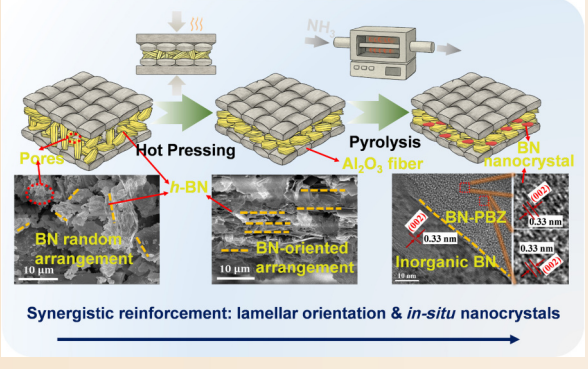

KEYWORDS: boron nitride-based composites; curing and pyrolysis of polyborazylene; lamellar alignment; mechanical properties

1 Introduction

As one of the critical components of aerospace vehicles, wave-transparent materials are responsible for enabling electromagnetic communication between the vehicle and ground stations, satellites, or other aircraft [1–3]. During flight missions, the radome/antenna window must ensure that electromagnetic waves can effectively pass through the material to maintain stable communication. In addition, since aerospace vehicles are subjected to high-speed flight, intense vibrations, extreme temperatures, and impact loads, radome/antenna windows must also possess excellent structural strength and environmental adaptability. Wave-transparent materials have evolved from organic materials [4], oxide ceramics [5], and nitride ceramics [6] to high-performance ceramic matrix composites. Nevertheless, challenges remain, including the trade-off between dielectric and mechanical properties, inadequate high-temperature resistance, and limited broadband adaptability and environmental stability.

Hexagonal boron nitride (*h*-BN) ceramics exhibit outstanding mechanical strength, dielectric properties, thermal shock resistance, and decomposition temperatures approaching 3000 °C in nitrogen or inert atmospheres [7–10]. These attributes have positioned *h*-BN ceramics as promising candidates for next-generation high-temperature wave-transparent materials, attracting growing research interest worldwide. However, due to their intrinsic brittleness, multiphase BN ceramics are prone to microcrack formation and propagation during the processing and service of large-scale components, especially under harsh operating conditions, which can result in catastrophic failure. To overcome these limitations, fiber-reinforced ceramic matrix composites (FCMCs) have emerged as leading alternatives, offering superior mechanical performance, high damage tolerance,

[1] Institute for Advanced Ceramics, School of Materials Science and Engineering, Harbin Institute of Technology, Harbin 150001, China. [2] Key Laboratory of Advanced Structural-Functional Integration Materials and Green Manufacturing Technology, Harbin Institute of Technology, Harbin 150001, China. [3] International Joint Laboratory of Advanced Nanomaterials of Heilongjiang Province, College of Materials Science and Chemical Engineering, Harbin Engineering University, Harbin 150001, China. [4] College of Environmental and Safety Engineering, Shenyang University of Chemical Technology, Shenyang 110000, China. [5] School of Materials Science and Engineering, Harbin Institute of Technology (Shenzhen), Shenzhen 518055, China.

✉ Corresponding authors. E-mail: D. Cai, caidelong@139.com; D. Jia, dcjia@hit.edu.cn

Received: October 25, 2025; Revised: December 17, 2025; Accepted: January 6, 2026

© The Author(s) 2026. This is an open access article under the terms of the Creative Commons Attribution 4.0 International License (CC BY 4.0, http://creativecommons.org/licenses/by/4.0/).

and scalability for complex geometries. Various wave-transparent FCMCs have been successfully developed, including Si_3N_{4f}/BN [11], SiO_{2f}/Si_3N_4-BN [12], and BN_f/BN [13]. For example, the bending strength retention of BN_f/BN composites at 1000 °C is 67.3%.

Al_2O_3 fibers exhibit a high melting point of 2050 °C and a boiling point of 2980 °C while maintaining excellent mechanical properties even in air at 1650 °C. Compared with other fibers, Al_2O_3 fibers possess high surface activity and outstanding resistance to high temperatures and corrosion, making them a material with exceptional comprehensive performance [14–16]. Therefore, composites prepared by combining Al_2O_3 fibers with a BN matrix are expected to exhibit superior overall performance. However, systematic studies on such materials remain relatively limited to date. The fabrication of Al_2O_{3f}/BN composites typically relies on hot pressing [17], CVI [18], and PIP processes [19], but all are constrained by the trade-off between densification, fiber integrity, and efficiency. Hot-pressing can enhance densification under high temperature and pressure, yet it causes abnormal grain growth in Al_2O_3 fibers, leading to strength degradation, while the need for high pressure to densify the layered BN structure further induces fiber fracture. CVI, although capable of protecting fibers under low-temperature and pressure-free conditions, suffers from surface-preferential deposition, resulting in long processing cycles, high porosity, and insufficient strength.

Currently, polymer infiltration and pyrolysis (PIP) and chemical vapor infiltration (CVI) have emerged as effective approaches for the fabrication of fiber-reinforced nitride ceramic matrix composites, demonstrating considerable potential for structural applications [20,21]. Nevertheless, critical challenges remain for established fabrication routes. For instance, CVI typically suffers from long deposition cycles (often > 100 h) and surface crusting effects [18]. Similarly, conventional PIP requires multiple repetitive cycles to eliminate residual porosity. As reported by Ma *et al.* [22] and Chen [23], fabricating dense nitride composites often necessitates 10–12 infiltration–pyrolysis cycles, which inevitably prolongs the fabrication period, increases energy consumption, and risks fiber damage due to repeated thermal shocks.

To address the aforementioned limitations, this study proposes a novel single-cycle densification strategy that synergizes liquid-phase precursor infiltration with texture design. Distinct from the multicycle nature of traditional PIP processes, our approach employs PBZ as a reactive liquid binder. The excellent low-temperature fluidity of PBZ facilitates the rearrangement of *h*-BN lamellae under pressure, enabling a "layer-stacking and hot-pressing" process that achieves high densification in a single step. Consequently, this route not only circumvents the time-consuming repetitive cycles associated with conventional PIP but also mitigates the issue of uneven matrix distribution common in mechanical blending. This offers a significantly more efficient pathway for the manufacturing of high-performance Al_2O_{3f}/BN composites. Specifically, this study investigates the critical influence of the curing process on the preferred orientation of *h*-BN lamellae, the microstructural evolution of the matrix, and the mechanical performance of the resulting composites. By leveraging the preferential alignment of lamellar BN structures during processing, matrix densification is promoted, and porosity is effectively reduced, thereby markedly shortening the overall fabrication cycle. This strategy not only enhances the mechanical properties and processing efficiency of Al_2O_{3f}/BN composites but also provides a scalable technical route for high-performance ceramic matrix composites, holding significant scientific and engineering value.

2 Experimental

2.1 Manufacturing process

The fabrication process of Al_2O_{3f}/BN composites is illustrated in Fig. 1. Al_2O_3 fiber cloth (Al_2O_3 content: 72 wt%, areal density: 400 g/m^2, satin weave; supplied by Shanghai Rongrong New Material Technology Co., Ltd., China) was selected as the reinforcement. Prior to processing, the sizing agent on the fiber surface is removed to enhance the wettability between the composite slurry and the fibers during subsequent steps and to prevent undesired reactions between the sizing agent and the matrix. Specifically, the cut fiber cloth was placed in a clean alumina crucible and heated in a muffle furnace at 600 °C for 2 h, followed by furnace cooling to room temperature.

Preparation of composite slurry: A specified amount of *h*-BN powder (d_{50} = 0.5 μm, 99% purity, Suzhou Nutpool Materials Technology Co., Ltd., China) was mixed with a liquid-phase PBZ solution (supplied by Shenyang University of Chemical

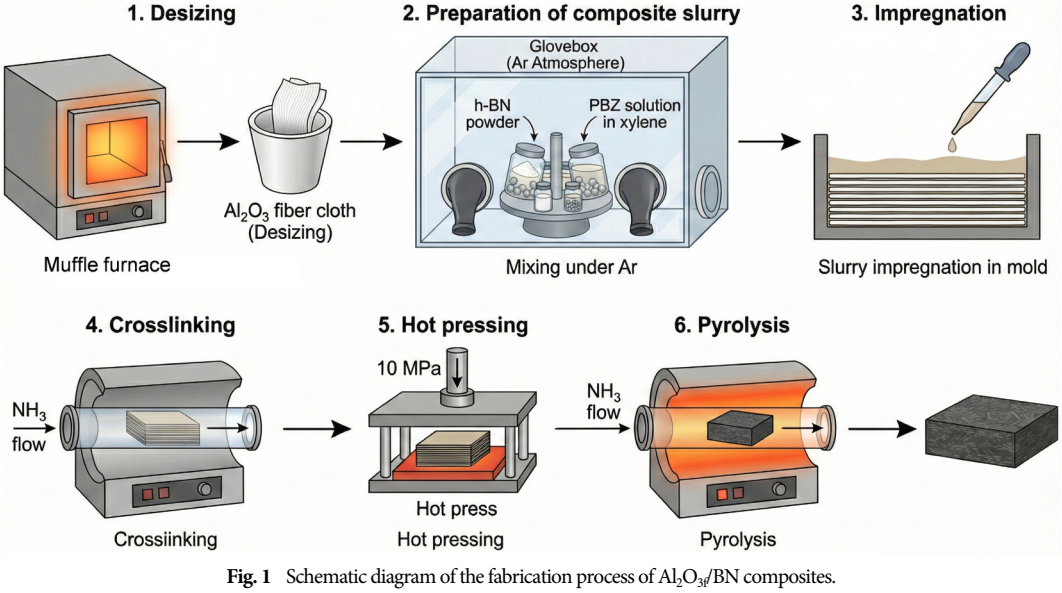

Fig. 1 Schematic diagram of the fabrication process of Al_2O_{3f}/BN composites.

Technology, China; purity > 99%; dissolved in xylene with a solid content of ~40 wt%; curing temperature range: 120–500 °C). The mixture was subsequently milled in a planetary ball mill for 8 h at a ball-to-powder weight ratio of 4 : 1. This results in an organic–inorganic composite slurry. To prevent oxidation of the PBZ during milling, the materials are loaded and processed in an argon-filled glovebox, ensuring that the entire mixing procedure is carried out under an inert Ar atmosphere.

The desized Al_2O_3 fiber cloth is uniformly impregnated with the composite slurry and layer-stacked in a mold according to the desired composite thickness. The layered preform and mold are placed in a tubular furnace, where crosslinking of the composite slurry is performed under a flowing ammonia atmosphere. The temperature was set at 150–500 °C to study the effect of curing temperature on the microstructure and mechanical properties of the composites.

Hot pressing: The cross-linked composites were consolidated using a flat-plate hot press. The process was conducted at 180 °C under a uniform uniaxial pressure of 10 MPa to ensure structural integrity and densification.

Pyrolysis: The hot-pressed composites were subjected to pyrolysis in a tubular furnace under an ammonia atmosphere. The samples were heated to 900 °C at a rate of 3 °C/min and held at this temperature for 2 h.

2.2 Characterizations

The pyrolysis behavior of PBZ was investigated by thermogravimetry–differential scanning calorimetry (TG-DSC) using an STA449F3 coupled with a QMS403D (Netzsch, Germany). The measurement was conducted from room temperature to 1550 °C at a heating rate of 10 °C/min under a nitrogen atmosphere. The volume density of the Al_2O_{3f}/BN composite specimens was measured in distilled water by the Archimedes principle (DV314C) at room temperature. The pore structure of the Al_2O_{3f}/BN composites was quantitatively characterized using mercury intrusion porosimetry (AutoPore V 9620, Micromeritics, USA). This analysis was employed to determine the calculated porosity, average pore diameter, and distribution of incremental pore volume as a function of pore diameter, providing insight into the microstructural evolution at different curing temperatures. X-ray diffractometry (Panalytical, the Netherlands) with Cu-Kα radiation was employed to characterize the phase composition and texture degree of the interlayer and cross-section of the Al_2O_{3f}/BN composite ceramics. Scanning electron microscopy (MAGNA, TESCAN, Czech Republic) was used to observe the cross-sectional morphology of the composites, the degree of weaving of the BN matrix, and the crack extension paths. The microstructure and elemental distribution of the composites were characterized using a transmission electron microscope (Talos F200X, FEI, USA). TEM specimens were prepared using a focused ion beam (FIB) system.

Bending strength was measured on samples with dimensions of 3 mm × 4 mm × 36 mm by the three-point bending method with the loading direction perpendicular to the lamination direction using a 30 mm span flexure fixture and a cross-head speed of 0.5 mm/min in an ambient temperature environment. The elastic modulus of the composite samples was measured at room temperature by means of a pulsed excitation technique (RDFA, IMCE, Belgium). The dimensions of the samples were 3 mm × 4 mm × 36 mm. The bending strength and elastic modulus were averaged over 4–6 measurements conducted under identical conditions.

3 Results and discussion

3.1 Thermal pyrolysis behavior of polyborazylene

To investigate the thermal behavior of PBZ during the preparation of composites, TG–DSC measurements were carried out under a nitrogen atmosphere, and the results are presented in Fig. 2. The pyrolysis process can be divided into three distinct stages, ultimately yielding a ceramic residue of approximately 30%. Stage I (room temperature–200 °C). In the low-temperature region, the TG curve exhibits a sharp weight loss of ~50%, while the DSC curve is dominated by endothermic signals. This behavior is primarily ascribed to the volatilization of residual solvents and low-molecular-weight species, accompanied by endothermic softening processes. A weak exothermic signal emerges near 150–200 °C, indicating the onset of dehydrocoupling between B–H and N–H groups, leading to partial B–N bond formation and the initiation of crosslinking/curing within the network.

Stage II (200–700 °C). In the intermediate temperature range, the TG curve declines gradually with an additional weight loss of ~20%. A broad exothermic peak appears at 200–300 °C, corresponding to further dehydrogenation, deamination, and enhanced crosslinking. Between 300 and 700 °C, the DSC curve progressively returns to the baseline with a slight endothermic shift, suggesting the elimination of organic side groups and the progressive development of an amorphous BN-based network, accompanied by the release of minor gaseous byproducts.

Stage III (700–1550 °C). At elevated temperatures, the TG curve continues to decrease slowly, stabilizing at a residual mass of ~30%. A broad endothermic domain emerges in the DSC curve, reaching a maximum at ~1130 °C, which is associated with structural rearrangement of the amorphous matrix and the onset of ordering toward a layered BN framework. Upon further heating to 1100–1500 °C, the DSC signal gradually diminishes with a slight exothermic shoulder, indicative of ordering and incipient crystallization of the BN layers. In summary, the pyrolysis of PBZ under nitrogen follows a typical transformation pathway characterized by low-temperature volatilization, progressive crosslinking/curing, and high-temperature framework rearrangement leading to structural ordering.

3.2 Microstructure of Al_2O_{3f}/BN composites

Figure 3 illustrates the cross-sectional morphologies, fiber volume fraction, bulk density, and pore structure evolution of Al_2O_{3f}/BN

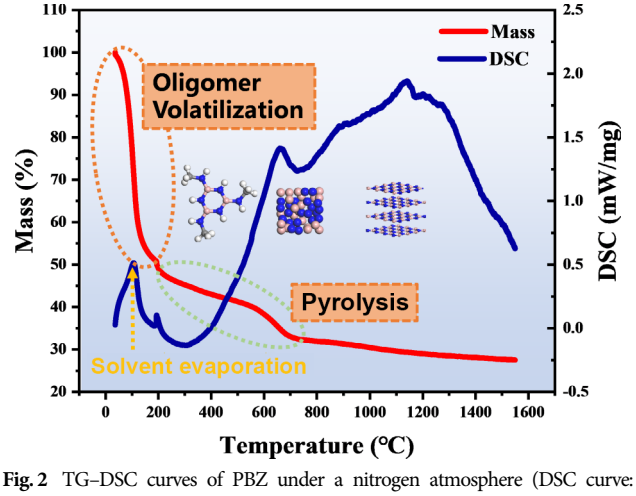

Fig. 2 TG–DSC curves of PBZ under a nitrogen atmosphere (DSC curve: exothermic downward, endothermic upward).

清華大学出版社 Tsinghua University Press | SciOpen

composites cured at different temperatures. Figs. 3(a)–3(e) presents cross-sectional SEM images of composites cured at 150–500 °C. It is evident that the curing temperature exerts a decisive influence on the matrix distribution and pore morphology. At 150 °C, the PBZ precursor is insufficiently cross-linked, and the slurry retains high fluidity. During hot pressing, part of the slurry is extruded from the prepreg layers, resulting in inadequate matrix retention, large and irregular pores, and insufficient filling between pore walls. When the curing temperature is increased to 200 °C, the PBZ precursor undergoes sufficient cross-linking, reducing slurry flowability to a moderate level. As a result, the slurry is effectively retained within fiber interspaces under pressure and uniformly fills interlayer voids. At this stage, the number of pores decreases significantly, and interlayer bonding becomes tighter, indicating a higher degree of densification. Upon further increasing the temperature to 300 °C and above, the PBZ precursor nearly loses all flowability, hindering its infiltration into fiber bundles. In addition, initial pyrolysis occurs, leading to matrix shrinkage and structural rearrangement, accompanied by the formation of new pores and microcracks. These defects cannot be completely eliminated under hot pressing, resulting in an increase in pore number and size. By 500 °C, the interlayer pores are significantly enlarged, the matrix distribution becomes uneven, and the overall structure appears loose.

Figure 3(f) shows the variation in the fiber volume fraction with curing temperature. The fiber volume fraction (V_f) was calculated using Eq. (1):

$$V_f = \frac{n \cdot S \cdot \sigma}{\rho_f \cdot V_c} \times 100\% \quad (1)$$

where n is the number of fiber layers, S is the area of the fiber cloth, σ is the areal density (400 g/m^2), ρ_f is the density of the Al_2O_3 fiber, and V_c is the measured volume of the composite.

The fiber content decreases continuously as the curing temperature increases. This is attributed to the progressive solidification and greater retention of the matrix at elevated curing temperatures, which increases the relative matrix fraction and reduces the fiber fraction. Figure 3(g) presents the bulk density curve, which exhibits a "first increase then decrease" trend. At 150 °C, severe matrix loss and high porosity lead to a low overall density. When the curing temperature rises to 200 °C, sufficient cross-linking of the PBZ precursor allows the slurry to effectively infiltrate the composite, significantly reducing pores and achieving optimal densification, with the bulk density reaching its maximum. As the curing temperature further increases to 300–500 °C, slurry flowability is gradually lost. Although the matrix content increases, fiber interspaces cannot be fully infiltrated. Considering that the theoretical density of alumina fibers (3.9 g/cm^3) is much higher than that of the BN matrix (~2.2 g/cm^3), the reduction in fiber proportion directly decreases the overall composite density. Moreover, matrix shrinkage and gas evolution during pyrolysis introduce additional pores, further lowering the density.

Figure 3(h) displays the variations in porosity and average pore size with curing temperature. Both reach their minimum values at

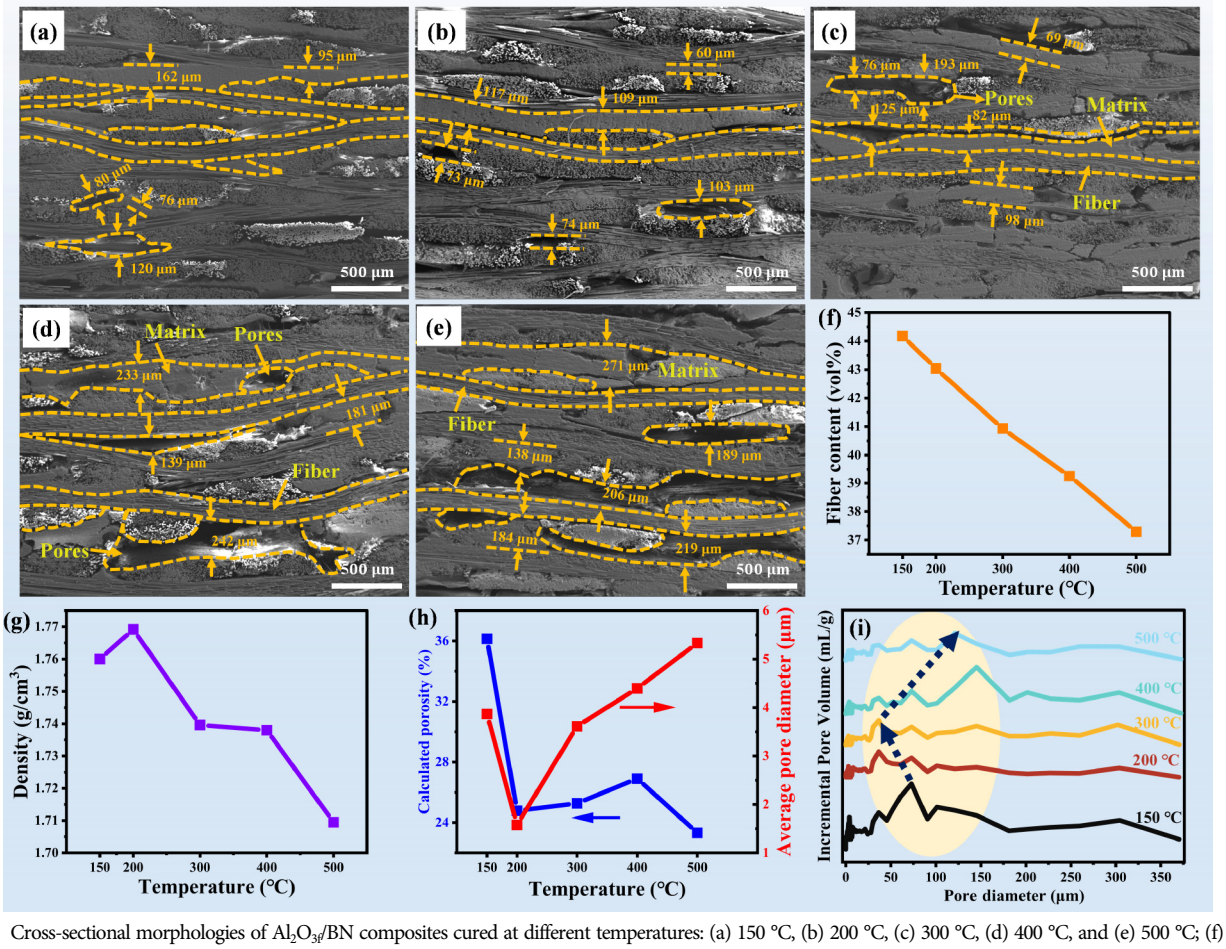

Fig. 3 Cross-sectional morphologies of Al_2O_{3f}/BN composites cured at different temperatures: (a) 150 °C, (b) 200 °C, (c) 300 °C, (d) 400 °C, and (e) 500 °C; (f) fiber content of the composites at various curing temperatures; (g) bulk density of the composites; (h) porosity and average pore size; and (i) pore size distribution of the composites determined by the mercury intrusion method.

200 °C, indicating optimal pore closure and the most uniform pore distribution. At 300 °C and above, the porosity and average pore size increase again, suggesting that matrix shrinkage and decomposition at high temperatures generate additional pore defects. Figure 3(i) shows the pore size distribution curves obtained by mercury intrusion porosimetry, which further verify the pore evolution with curing temperature. At 150 °C, the distribution is skewed toward large pore sizes, indicating numerous unfilled interlayer voids. At 200 °C, the distribution narrows significantly, reflecting the effective filling of large pores and the densest pore structure. As the curing temperature increases to 300–500 °C, the distribution broadens again, with a noticeable increase in small and medium pores and the persistence of some large pores, confirming that matrix shrinkage and gas release at higher temperatures induce new pores and accumulate defects.

In summary, curing temperature has a pronounced influence on both the microstructure and macroscopic properties of Al_2O_{3f}/BN composites. At 200 °C, the balance between the matrix and fibers is most favorable, with porosity and average pore size reaching their lowest values, resulting in optimal densification and a uniform pore structure. In contrast, excessively low or high curing temperatures lead to matrix loss or pyrolysis-induced defects, which reduce the degree of densification and ultimately compromise the overall performance of the composites.

The matrix morphologies of the Al_2O_{3f}/BN composites prepared at different curing temperatures are shown in Figs. 4(a), 4(c), 4(e), 4(g), and 4(i). The composites exhibit a distinct lamellar structure. Consistent with the XRD analysis, when the curing temperature is in the range of 150–200 °C, the *h*-BN grains in the composites tend to align perpendicular to the hot-pressing direction. As the curing temperature increases, the degree of *h*-BN grain orientation gradually weakens. Microscopic observations reveal that the orientation of *h*-BN ceramic grains is most pronounced at a curing temperature of 200 °C. When the curing temperature is further increased, the reduced liquid-phase content during the hot-pressing process limits the mobility and rearrangement of particles, leading to a decline in the degree of orientation.

The XRD patterns of the surface and cross-section of the Al_2O_{3f}/BN composites cured at different temperatures are shown in Figs. 4(b), 4(d), 4(f), 4(h), and 4(j). The composites exhibit diffraction peaks corresponding to *h*-BN, γ-Al_2O_3, and mullite phases. Notably, the presence of the mullite phase is attributed to the *in situ* reaction between the γ-Al_2O_3 and amorphous SiO_2 components within the fibers. Apart from this intrafiber phase evolution, the diffraction patterns remain relatively consistent across the temperature range of 150–500 °C, indicating that the macroscopic structural evolution is primarily governed by the pyrolysis and consolidation of the PBZ precursor rather than new interfacial chemical reactions.

In the XRD patterns measured from the composite surface, the diffraction intensities of the *h*-BN (002) and (004) planes are significantly higher than those observed in the cross-section. Conversely, the intensities of the (100) and (110) planes are markedly lower on the surface. Notably, this anisotropic diffraction behavior gradually diminishes as the curing temperature increases.

These results suggest that lower curing temperatures promote the preferential orientation of *h*-BN crystallites, with their *c*-axis aligned perpendicular to the pressing direction. However, as the curing temperature increases, this orientation becomes less pronounced, indicating that higher curing temperatures hinder the development of highly oriented *h*-BN structures. Moreover, the *c*-axis of the *h*-BN grains tends to rotate toward alignment with the hot-pressing direction.

TEM observation (Fig. 4(k)) further reveals the orientation characteristics of the BN matrix. It is clearly observed that the added inorganic *h*-BN lamellae are aligned perpendicular to the hot-pressing direction, while the BN converted from PBZ fills the

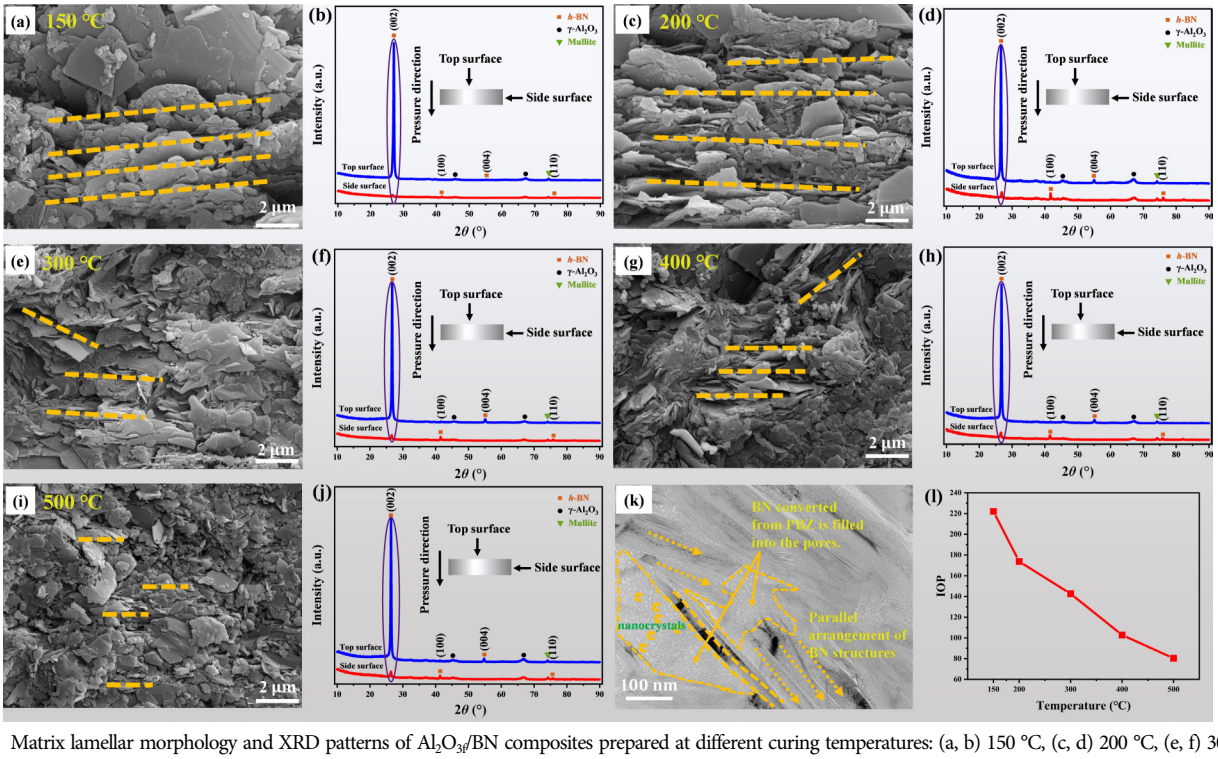

Fig. 4 Matrix lamellar morphology and XRD patterns of Al_2O_{3f}/BN composites prepared at different curing temperatures: (a, b) 150 °C, (c, d) 200 °C, (e, f) 300 °C, (g, h) 400 °C, and (i, j) 500 °C; (h) oriented structure of the BN matrix in Al_2O_{3f}/BN composites observed by TEM; (i) IOP calculation of composite.

pores formed between the *h*-BN layers. Such a lamellar orientation structure is considered an important structural feature of the BN matrix and has a direct influence on the mechanical properties and fracture behavior of the composites.

To quantitatively evaluate the effect of curing temperature on the orientation degree of *h*-BN grains in the composite, the index of orientation preference (IOP) [24] of *h*-BN crystallites was calculated using Eq. (2):

$$\mathrm{IOP} = \begin{cases} \dfrac{(I_{100}/I_{002})_{\mathrm{top}}}{(I'_{100}/I'_{002})_{\mathrm{side}}}, & (I_{100}/I_{002})_{\mathrm{top}} > \left(I'_{100}/I'_{002}\right)_{\mathrm{side}} \\ -\dfrac{\left(I'_{100}/I'_{002}\right)_{\mathrm{side}}}{(I_{100}/I_{002})_{\mathrm{top}}}, & (I_{100}/I_{002})_{\mathrm{top}} < \left(I'_{100}/I'_{002}\right)_{\mathrm{side}} \end{cases} \quad (2)$$

where I_{hkl} represents the intensity of diffraction peaks at surface-associated crystal faces, and I'_{hkl} represents the diffraction peak intensities of cross-sectionally correlated crystalline surfaces.

When the IOP equals ±1, the *h*-BN grains are randomly oriented. An IOP greater than 1 suggests that the *c*-axis of the *h*-BN crystallites tends to align perpendicular to the hot-pressing direction, while an IOP less than –1 indicates that the *c*-axis tends to align parallel to the hot-pressing direction. The IOP values of Al_2O_{3f}/BN composites cured at different temperatures are shown in Fig. 4(i). As the curing temperature increases from 150 to 500 °C, the IOP values decrease from 222.07 to 80.36, indicating that lower curing temperatures are more favorable for the oriented alignment of *h*-BN grains. This trend is mainly attributed to the fact that lower curing temperatures result in higher slurry fluidity. Under such conditions, *h*-BN particles are more likely to undergo oriented alignment in the liquid-phase environment during hot pressing.

Figure 5 presents the TEM characterization of Al_2O_{3f}/BN composites cured at 200 °C and subsequently pyrolyzed at 900 °C. As shown in the low-magnification TEM image (Fig. 5(a)), *h*-BN and BN-PBZ are uniformly distributed within the matrix. A small number of pores can still be observed at the Al_2O_3 fiber/matrix interface, which are mainly attributed to gas release during the pyrolysis of the precursor. Nevertheless, the interfacial contour remains relatively clear, indicating that the fabrication process effectively suppressed the formation of large macroscopic voids. The SAED pattern of the fiber (Fig. 5(c)) further confirms that it retains the structural characteristics of γ-Al_2O_3, with typical diffraction rings corresponding to the (400) and (440) planes. This result demonstrates that the Al_2O_3 fibers maintained their crystalline structure throughout the entire process without undergoing significant phase transformation, which plays a critical

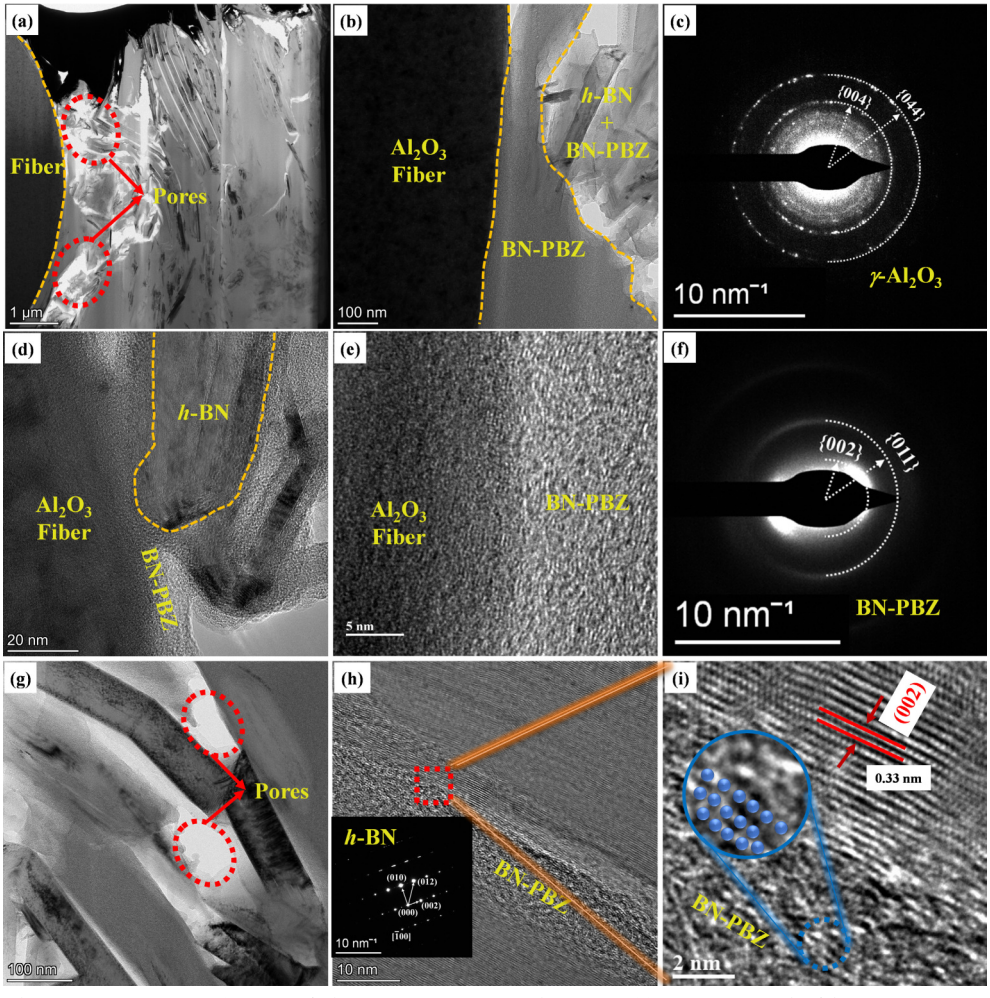

Fig. 5 Transmission electron microscopy (TEM) images of Al_2O_{3f}/BN composites cured at 200 °C. (a) TEM micrograph of the composite prepared by FIB; (b) TEM micrograph of the interface between Al_2O_3 fibers and the BN matrix; (c) selected-area electron diffraction (SAED) pattern of Al_2O_3 fibers; (d) high-resolution TEM (HRTEM) image of the Al_2O_3 fiber/BN matrix interface; (e) HRTEM image of the Al_2O_3 fiber edge; (f) SAED pattern of BN-PBZ; (g) TEM image of the BN matrix; (h) HRTEM image of the *h*-BN/BN-PBZ interface, with inset showing the SAED pattern of *h*-BN; (i) enlarged HRTEM image of the *h*-BN/BN-PBZ interface.

role in ensuring the stability of the reinforcing phase in the composites.

In the high-resolution TEM image of the interfacial region (Fig. 5(d)), a thin transition layer can be observed between the fiber and the BN matrix. This layer is primarily composed of BN derived from PBZ pyrolysis. The HRTEM image (Fig. 5(e)) clearly reveals the contrast between the ordered lattice of Al_2O_3 and the disordered BN-PBZ structure at the interface, further highlighting their distinct structural features at the nanoscale. Meanwhile, the SAED pattern of the BN-PBZ matrix near the interface (Fig. 5(f)) shows diffuse rings corresponding to the (002) and (011) planes, indicating that the pyrolyzed BN predominantly exhibits a turbostratic structure with relatively low crystallinity. It is worth noting, however, that nanoscale crystallites are locally precipitated within these disordered regions, suggesting that BN-PBZ is not entirely amorphous but partially undergoes structural ordering during pyrolysis. These nanocrystals, with their more regular layered structures, can serve as load-transfer nodes at the nanoscale, thereby enhancing the mechanical performance of the composites. This phenomenon indicates that although the pyrolyzed BN is generally disordered, the presence of nanocrystals provides an additional microscopic reinforcement mechanism.

The overall morphology of the BN matrix is illustrated in Fig. 5(g), where a small amount of porosity is observed, which is directly associated with gas release during the 900 °C pyrolysis process. Although the presence of pores reduces the overall densification of the matrix, it does not compromise the structural continuity. A closer view of the interface (Fig. 5(h)) reveals that highly ordered *h*-BN layers are in intimate contact with disordered BN-PBZ, forming a distinct interfacial transition region. The inset SAED pattern corresponds to *h*-BN, exhibiting sharp diffraction spots, confirming its high crystallinity. Finally, the enlarged HRTEM image (Fig. 5(i)) resolves well-defined (002) lattice fringes with an interlayer spacing of approximately 0.33 nm, which can be assigned to the inorganic *h*-BN filler, indicating that it maintains high crystallinity throughout the process. In contrast, the BN-PBZ in the lower-left region of the image remains disordered, with only sporadic nanocrystalline fringes observed. This further confirms the "dual structural characteristics" of pyrolyzed BN: predominantly turbostratic at the macroscale, while containing a small fraction of nanocrystalline domains at the nanoscale.

Figure 6 presents the HAADF-STEM image and corresponding EDS elemental analyses of the Al_2O_{3f}/BN composite. Three representative regions (A1–A3) were selected from the HAADF image for quantitative EDS analysis to elucidate the compositional characteristics of the fiber region, the interfacial transition region, and the BN matrix. The elemental mapping on the right further illustrates the spatial distribution of B, C, N, O, Al, and Si, revealing the multiphase composition of the composite.

In region A1, the EDS analysis clearly shows that Al, Si, and O are the major elements with relatively high contents. Based on the compositional ratio, this region corresponds to the Al_2O_3 fiber. Overall, the elemental features of this region are consistent with those of γ-Al_2O_3, indicating that the fibers retain their compositional stability within the composite.

In region A2, the spectrum reveals the coexistence of Al, Si, and O together with B and N. The compositional characteristics here are distinct from those of either the fiber body or the BN matrix, suggesting that A2 represents the interfacial transition zone. The presence of Al–Si–O elements indicates the influence of the fiber, while B and N reflect the formation of BN derived from the precursor.

In region A3, B and N are the dominant elements,

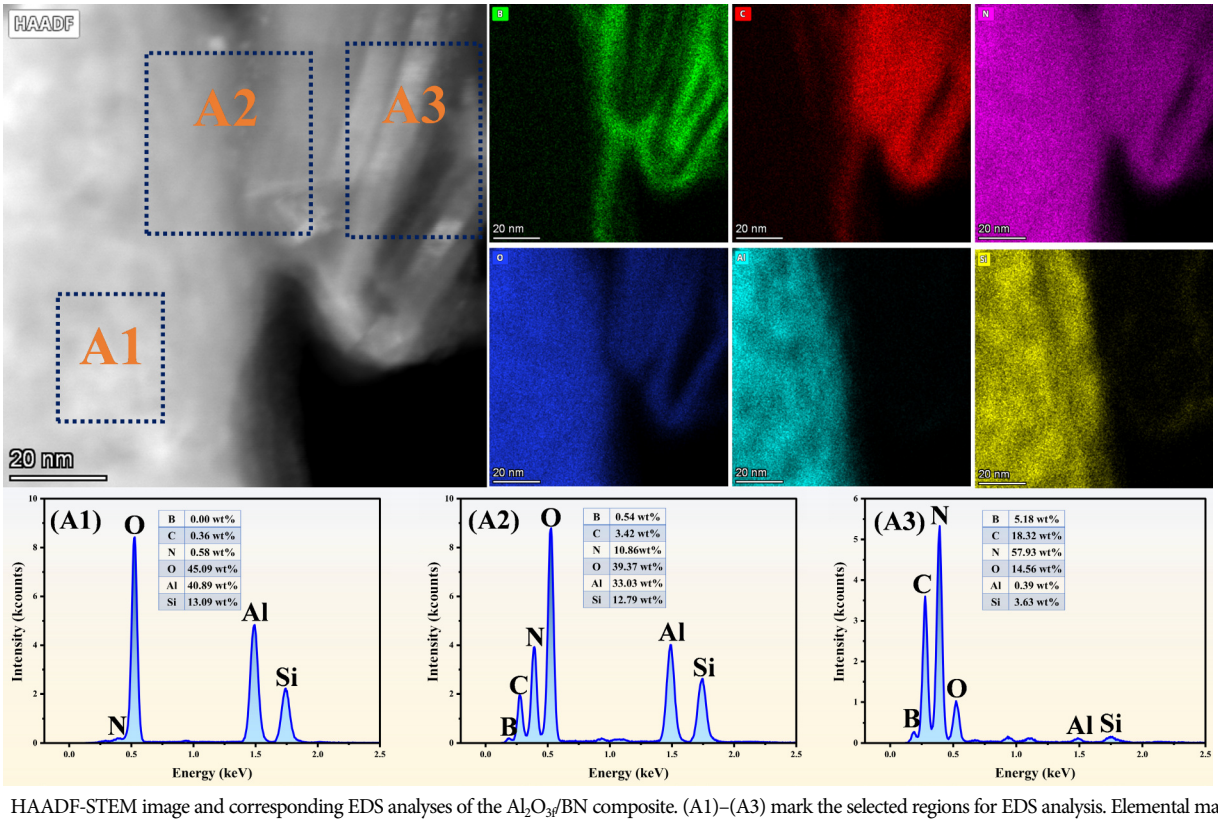

Fig. 6 HAADF-STEM image and corresponding EDS analyses of the Al_2O_{3f}/BN composite. (A1)–(A3) mark the selected regions for EDS analysis. Elemental mapping of (B) B, (C) C, (N) N, (O) O, (Al) Al, and (Si) Si is shown, demonstrating the spatial distribution of the major constituents. (A1)–(A3) EDS spectra and corresponding elemental compositions (in wt%).

accompanied by minor amounts of C and O. The relatively high B and N contents confirm that this region corresponds to the BN matrix. The trace amount of C is attributed to the incomplete conversion of residual carbon from the precursor, while the small amount of O may originate from oxygen introduced via PBZ or slight surface oxidation. Compared with regions A1 and A2, the compositional profile of region A3 is more homogeneous, reflecting the principal chemical composition of the BN matrix.

3.3 Mechanical properties of Al_2O_{3f}/BN composites

The bending strength and elastic modulus of the Al_2O_{3f}/BN composites, measured perpendicular to the ply-stacking direction under different curing temperatures, are shown in Fig. 7(a). As the curing temperature increases from 150 to 200 °C, both the bending strength and elastic modulus of the composite significantly improve. As the curing temperature increases from 150 to 200 °C, the mechanical performance of the composite shows a sharp upward trend. At the optimal curing temperature of 200 °C, the composites exhibit a bending strength of 32.53± 2.71 MPa and an elastic modulus of 27.08±0.60 GPa. Quantitatively, this represents a significant improvement of approximately 50% compared to the samples cured at 150 °C (which exhibited a strength of ~21.66 MPa). This enhancement is directly correlated with the evolution of structural integrity: as the curing temperature was optimized, the porosity decreased from ~36.1% (at 150 °C) to a minimum of 24.8% (at 200 °C). This quantitative correlation confirms that the proposed 'single-cycle' route effectively mitigates the trade-off between porosity and strength, achieving high densification. However, when the curing temperature is further increased, both the bending strength and elastic modulus begin to decline. This variation in mechanical properties is closely related to changes in porosity and the composite microstructure [25]. As indicated by Eq. (3), porosity has a pronounced effect on the mechanical performance of ceramic materials.

$$\sigma = \sigma_0 \exp(-np) \tag{3}$$

where σ is the material strength, σ_0 represents the material strength when the porosity is zero, n is a constant, and p denotes the porosity.

Under the curing condition of 150 °C, the slurry tends to be extruded during the hot-pressing process, resulting in poor matrix

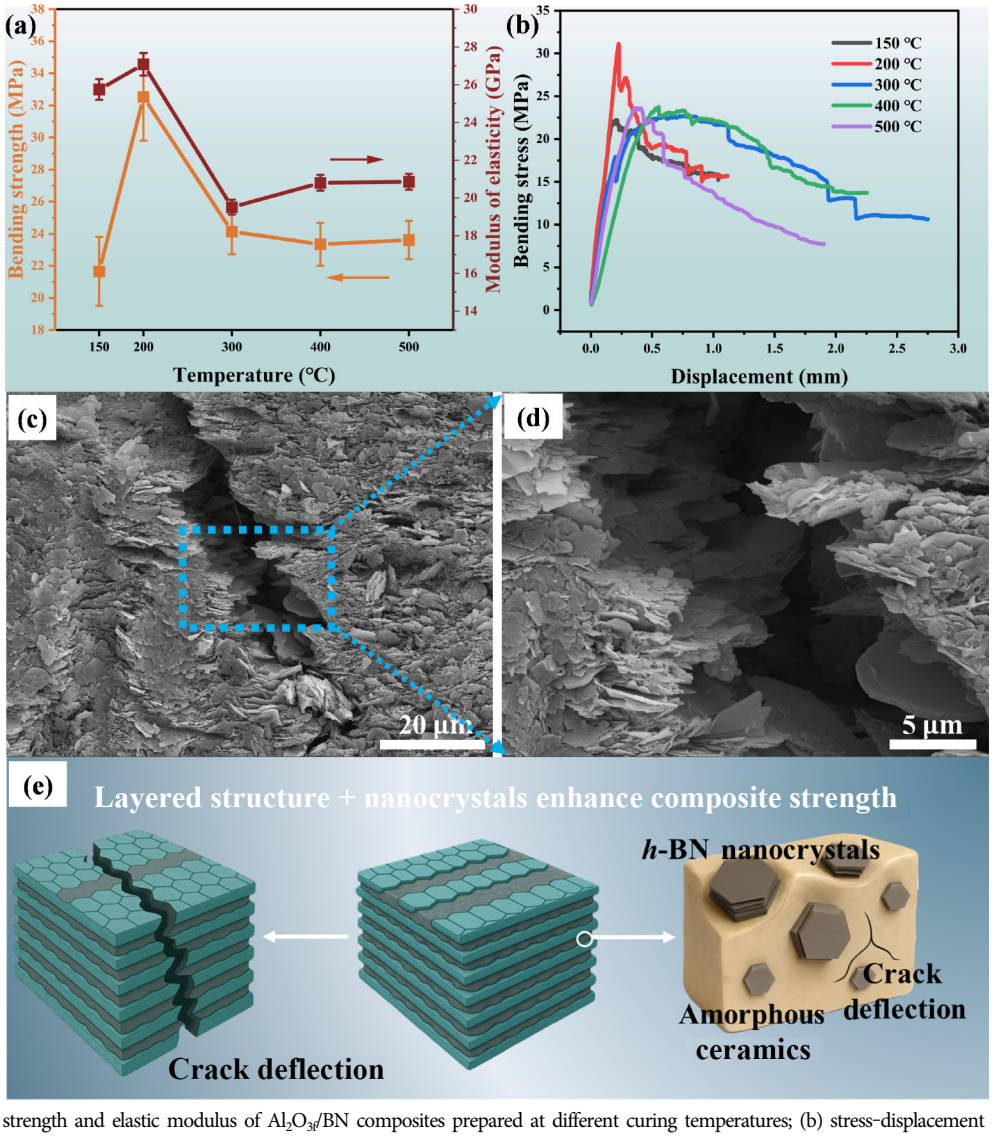

Fig. 7 (a) Bending strength and elastic modulus of Al_2O_{3f}/BN composites prepared at different curing temperatures; (b) stress-displacement curves of Al_2O_{3f}/BN composites prepared at different curing temperatures; (c, d) crack propagation morphology in the BN matrix of Al_2O_{3f}/BN composite materials; (e) dominant strengthening mechanisms in Al_2O_{3f}/BN composites.

filling between the fibers. This leads to a relatively high overall porosity and large pore size in the composite, causing insufficient densification and the formation of many interconnected pores. When the curing temperature is increased to 200 °C, the precursor undergoes moderate cross-linking, reducing slurry fluidity and allowing it to be well retained between fiber layers. This significantly decreases the number of internal pores, lowers the porosity to its minimum value, and results in a more uniform pore size distribution. The reduced porosity enhances the continuity and integrity of the composite matrix, thereby significantly improving the bending strength and elastic modulus and achieving optimal overall mechanical performance. However, as the curing temperature further rises to 300 °C and above, the precursor becomes fully cross-linked and loses flowability under hot pressing. This prevents the liquid phase from effectively promoting the oriented alignment of *h*-BN particles and densification, resulting in higher porosity and consequently poorer mechanical properties.

Additionally, the variation in the fiber volume fraction plays a critical role in determining the ultimate strength of the composites. As shown in Fig. 3(f), the content of Al_2O_3 fibers—which serve as the primary load-bearing skeleton—decreases linearly with increasing curing temperature due to the enhanced retention of the matrix. According to the rule of mixtures for composite materials, a reduction in the volume fraction of the high-strength reinforcement phase directly diminishes the material's load-bearing capacity. Therefore, the decline in bending strength and elastic modulus observed at curing temperatures above 200 °C is attributed to a synergistic negative effect: the increase in porosity acts as a defect center facilitating crack initiation, while the simultaneous decrease in fiber volume fraction reduces the effective structural reinforcement.

It is worth noting that while the bending strength of 32.53 MPa is lower than that of fully dense structural ceramics, it is comparable to established porous wave-transparent materials used in engineering. For instance, Wang *et al.* [26] reported a bending strength of 30.7 MPa for pressureless sintered *h*-BN ceramics, and porous fused silica ceramics widely used for radomes typically exhibit strengths in the range of 20–60 MPa depending on porosity [5]. This suggests that the prepared Al_2O_{3f}/BN composites possess sufficient structural integrity for secondary load-bearing components such as antenna windows while offering a significantly shorter fabrication cycle.

Figures 7(c) and 7(d) show the crack propagation morphology within the matrix of the Al_2O_{3f}/BN composites. Figure 7(c) presents a low-magnification SEM image revealing that cracks extend along the orientation direction of the *h*-BN lamellae. The crack paths are tortuous and irregular, lacking simple straight-through characteristics. During propagation in the BN matrix, cracks are significantly influenced by the oriented lamellar structure, causing frequent deflections and branching. This indicates that the internal lamellar architecture effectively promotes crack deflection and blunting, thereby impeding crack growth.

Such crack propagation behavior lengthens the crack path and increases the energy consumption during crack extension, which contributes to the enhancement of the composite's mechanical properties. Figure 7(d) is a magnified view of the region shown in Fig. 7(c), further revealing the microscopic features at the crack tip. It clearly shows pronounced branching, deflection, and extension of cracks between the lamellae, demonstrating the "lamellar energy dissipation mechanism" of the *h*-BN matrix in controlling crack propagation paths.

This interlaminar sliding and debonding effectively dissipate externally applied load energy, preventing rapid linear crack growth within the matrix. As a result, crack instability is delayed, leading to improved fracture toughness and resistance to crack propagation. Additionally, the crack propagation path is closely correlated with the orientation direction of the *h*-BN lamellae. Cracks must continuously change direction to circumvent the oriented lamellae, and this deflection behavior effectively slows the crack growth rate and increases the overall fracture energy of the composite. Therefore, the oriented lamellar structure of *h*-BN plays a critical role in the toughening mechanism of the material.

3.4 Densification mechanism of Al_2O_{3f}/BN composites

The densification mechanism of the Al_2O_{3f}/BN composite material is shown in Fig. 8. In the initial stage, the added *h*-BN lamellae are randomly distributed within the matrix, resulting in many pores and defects. After hot pressing, the applied pressure promotes the gradual alignment of *h*-BN lamellae perpendicular to the hot-pressing direction. Mechanistically, the liquid-phase PBZ serves as a lubricant, significantly reducing the interparticle friction between the rigid *h*-BN platelets. Under uniaxial pressure, the viscous flow of the liquid precursor generates shear stress, which imposes a torque on the high-aspect-ratio platelets. This torque facilitates the rotation of the platelets, forcing them to align perpendicular to the compression axis. This rearrangement significantly reduces the number of pores and improves the densification of the matrix. Subsequently, during high-temperature pyrolysis under an ammonia atmosphere, the PBZ precursor is converted into turbostratic BN, which fills the pores between the *h*-BN lamellae, thereby further enhancing the structural integrity and interlayer bonding of the matrix. More importantly, during pyrolysis, part of the PBZ-derived BN precipitates as nanocrystals. These nanocrystals act as load-transfer nodes at the nanoscale, effectively improving the mechanical performance of the composites. The final composite is thus composed of Al_2O_3 fibers as reinforcement, oriented *h*-BN lamellae, turbostratic BN filling the interlamellar pores, and locally precipitated nanocrystals.

The observed microstructural evolution confirms that hot pressing can effectively induce the orientational alignment of *h*-BN sheets. As shown by the high IOP value obtained at 200 °C (Fig. 4(i)), this significant orientation forces crack propagation deflection, thereby greatly increasing the fracture energy. Furthermore, *in situ* precipitated BN nanocrystals derived from PBZ act as key load transfer nodes. This synergistic mechanism combining macroscopic deflection and microscopic reinforcement is the main driving factor for improved bending strength. Therefore, the construction of this ordered-disorder hybrid structure optimizes the overall mechanical properties by maximizing energy dissipation through crack deflection and branching.

4 Conclusions

In this work, Al_2O_{3f}/BN composites were fabricated via layer-stacking, hot-pressing, and pyrolysis processes. This study systematically investigated the critical role of curing temperature in regulating matrix densification, pore structure, and mechanical performance. The main conclusions are summarized as follows:

(i) Densification mechanism: An "oriented lamellae–turbostratic filling–nanocrystal reinforcement" mechanism was identified. At lower curing temperatures, the PBZ precursor facilitated the oriented alignment of *h*-BN lamellae and effective pore filling. Subsequent high-temperature pyrolysis generated BN

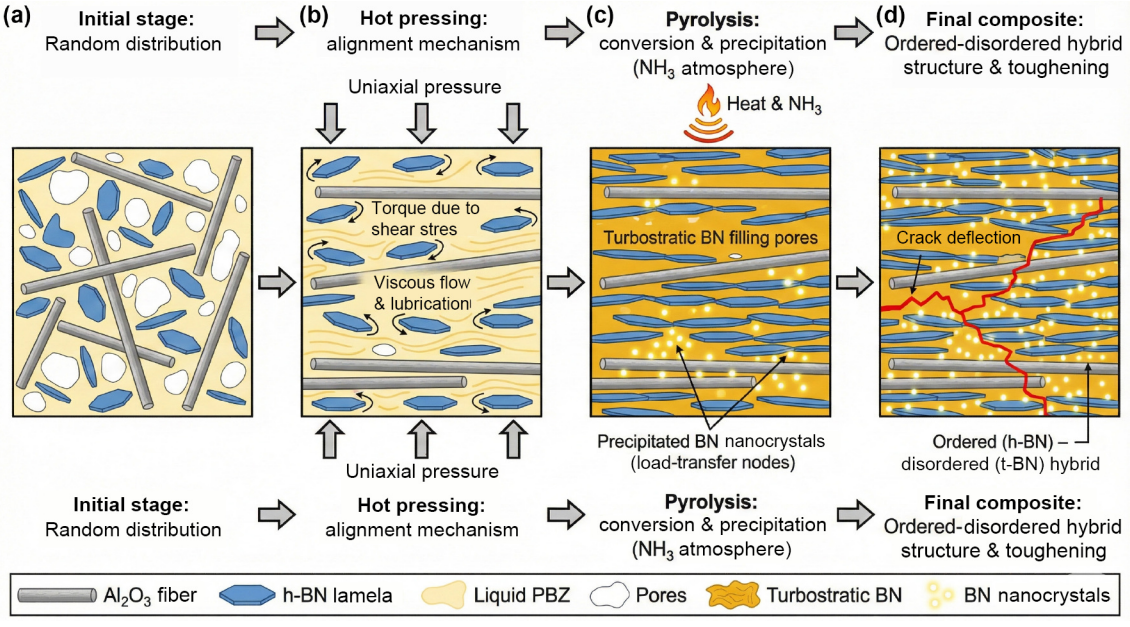

Fig. 8 Schematic diagram of the densification mechanism of the Al_2O_{3f}/BN composite.

nanocrystals, which strengthened the interfacial bonding and improved the load transfer efficiency.

(ii) Microstructural evolution: The curing temperature significantly influenced the microstructure. With the temperature increasing to 200 °C, the composite achieved optimal densification, balancing the degree of *h*-BN orientation with the matrix content. The apparent porosity reached a minimum value of 24.78% at this temperature.

(iii) Mechanical performance: The mechanical properties were maximized at a curing temperature of 200 °C, yielding a bending strength of 32.53±2.71 MPa and an elastic modulus of 27.08± 0.60 GPa. This represents an ~50% improvement in strength compared to samples cured at nonoptimal temperatures (e.g., 150 °C). This enhancement is attributed to the synergistic effect of crack deflection by oriented h-BN lamellae and energy dissipation by the PBZ pyrolysis products.

(iv) Application potential: Based on the optimized structural integrity and mechanical performance, the prepared Al_2O_{3f}/BN composites demonstrate promise for use as high-temperature wave-transparent materials. The findings provide a theoretical basis for optimizing the fabrication parameters of ceramic matrix composites for potential aerospace applications.

Acknowledgements

This work was supported by the National Key Research and Development Program of China (No. 2024YFB3714702), the National Natural Science Foundation of China (Nos. 52072088 and 52072089), the Natural Science Foundation of Heilongjiang Province (No. LH2023E061), and the Scientific and Technological Innovation Leading Talent of Harbin Manufacturing (No. 2022CXRCCG001).

Author contributions

Bo Wang: Writing—original draft. Delong Cai and Dechang Jia: Resources and methodology. Xiaoming Duan, Zhihua Yang, Daxin Li, Zhenxi Lu and Yu Zhou: Writing—review & editing.

Availability of data and materials

The data that support the findings of this study are available from the corresponding author upon reasonable request.

Competing interests

The authors have no competing interests to declare that are relevant to the content of this article.

References

[1] Zhang YB, Wang B, Du YA, *et al.* High crystallinity BN fiber derived from organic–inorganic hybrid BNNS/polyborazine precursor. *J Am Ceram Soc* 2025, **108**: e20439.

[2] Yang XJ, Li B, Li D, *et al.* High-temperature properties and interface evolution of silicon nitride fiber reinforced silica matrix wave-transparent composite materials. *J Eur Ceram Soc* 2019, **39**: 240–248.

[3] Duan XM, Yang ZH, Chen L, *et al.* Review on the properties of hexagonal boron nitride matrix composite ceramics. *J Eur Ceram Soc* 2016, **36**: 3725–3737.

[4] Tang L, Zhang JL, Tang YS, *et al.* Polymer matrix wave-transparent composites: A review. *J Mater Sci Technol* 2021, **75**: 225–251.

[5] Miao XG, Qu YR, Ghezzo F, *et al.* Fused silica ceramics and composites for radome applications. *Adv Mater Res* 2014, **900**: 123–129.

[6] Kandi KK, Thallapalli N, Chilakalapalli SPR. Development of silicon nitride-based ceramic radomes—A review. *Int J Appl Ceram Technol* 2015, **12**: 909–920.

[7] Wang ZG, Ge M, Yu SQ, *et al.* Microstructural evolution of polymer-derived hexagonal boron nitride fibres under high-temperature stretching. *J Adv Ceram* 2023, **12**: 1973–1988.

[8] Yang N, Kenion T, Xu SF, *et al.* Dielectric property characterization at high temperature (RT to 1000 ℃) of BN-based electromagnetic transparent materials for hypersonic applications. *Ceram Int* 2023, **49**: 11047–11059.

[9] Du YA, Wang B, Zhang YB, *et al.* Online preparation of high-quality BN coatings with atomic diffusion based on carbon-free water-soluble precursor. *J Adv Ceram* 2024, **13**: 272–281.

[10] Jiang LY, Pang SY, Yang C, *et al.* Preparation and oxidation behaviors of C/SiC-BN composites. *J Inorg Mater* 2024, **39**: 779.

[11] Zou CR, Li B, Liu K, *et al.* Microstructure and mechanical properties of Si_3N_4f/BN composites with BN interphase prepared by chemical vapor deposition of borazine. *J Eur Ceram Soc* 2020, **40**: 1139–1148.

[12] Jiang YG, Zhang CR, Cao F, *et al.* Fabrication of high performance 2.5D SiO_2f/Si_3N_4-BN composites for high-temperature application. *Adv Eng Mater* 2007, **9**: 114–116.

[13] Li D, Zhang CR, Li B, *et al.* Preparation and properties of unidirectional boron nitride fibre reinforced boron nitride matrix

composites via precursor infiltration and pyrolysis route. *Mater Sci Eng A* 2011, **528**: 8169–8173.
[14] Li WX, Ji XY, Gai K, *et al.* Regulating crystalline behavior to create fully crystallized α-Al_2O_3-mullite continuous ceramic fibers derived from the melt-spinning of polymer precursor. *Ceram Int* 2025, **51**: 7897–7905.
[15] Zhu CX, Zheng Z, Cao F, *et al.* High-temperature properties of Al_2O_3 /SiO_2 composites. *J Sol Gel Sci Technol* 2021, **97**: 63–70.
[16] Zhang HH, Zhang YM, Wang B, *et al.* Preparation and characterization of continuous alumina based fiber reinforced with orientated mullite whisker. *Chem Eng J* 2015, **268**: 109–115.
[17] Lee PY, Imai M, Yano T. Effects of sintering condition on mechanical properties of monazite-coated alumina-fiber/alumina-matrix composites fabricated by hot-pressing. *J Ceram Soc Japan* 2004, **112**: 29–34.
[18] Li JP, Cheng LF, Ye F, *et al.* Preparation and properties of BN fiber reinforced nitride mini-composites. *Rare Met Mater Eng* 2018, **47**: 2901–2908. (in Chinese)
[19] Li D, Li B, Zheng YY, *et al.* On the mechanical, thermophysical and dielectric properties of Nextel™ 440 fiber reinforced nitride matrix (N440/Nitride) composites. *Ceram Int* 2018, **44**: 6137–6143.
[20] Wang HL, Gao ST, Peng SM, *et al.* KD-S SiC_f/SiC composites with BN interface fabricated by polymer infiltration and pyrolysis process. *J Adv Ceram* 2018, **7**: 169–177.
[21] Gao Q, Hu P, Xun LC, *et al.* A scalable method allows for the rapid fabrication of C/SiC composites with excellent mechanical properties and ablation resistance. *J Adv Ceram* 2025, **14**: 9221162.
[22] Ma X, Liang YY, Qiu HP, *et al.* Preparation of high-performance 2D Si_3N_{4f}/SiBN ceramic matrix composites by precursor infiltration pyrolysis. *IOP Conf Ser: Mater Sci Eng* 2019, **678**: 012044.
[23] Chen WM. Study on preparation and properties of boron niride ceramic fibers derives from polymeric precursors and BN_f/BN composites. Ph.D. Thesis. Beijing (China): University of Chinese Academy of Sciences, 2012. (in Chinese)
[24] Niu B, Cai DL, Yang ZH, *et al.* Anisotropies in structure and properties of hot-press sintered h-BN-MAS composite ceramics: Effects of raw h-BN particle size. *J Eur Ceram Soc* 2019, **39**: 539–546.
[25] Jia DC, Song GM. *Properties of Inorganic Nonmetallic Materials*. Beijing (China): Science Press, 2008. (in Chinese)
[26] Wang TB, Jin CC, Yang J, *et al.* Physical and mechanical properties of hexagonal boron nitride ceramic fabricated by pressureless sintering without additive. *Adv Appl Ceram* 2015, **114**: 273–276.